

## Humidity control can compensate for the damage induced in protein crystals by alien solutions

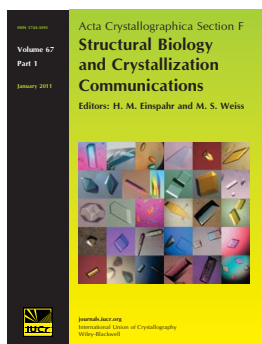
**C. Abad-Zapatero, R. Oliete, S. Rodriguez-Puente, J. Pous, L. Martinelli,  
M. E. Johnson and A. Guasch**

*Acta Cryst.* (2011). **F67**, 1300–1308

Copyright © International Union of Crystallography

Author(s) of this paper may load this reprint on their own web site or institutional repository provided that this cover page is retained. Republication of this article or its storage in electronic databases other than as specified above is not permitted without prior permission in writing from the IUCr.

For further information see <http://journals.iucr.org/services/authorrights.html>



*Acta Crystallographica Section F: Structural Biology and Crystallization Communications* is a rapid all-electronic journal, which provides a home for short communications on the crystallization and structure of biological macromolecules. Structures determined through structural genomics initiatives or from iterative studies such as those used in the pharmaceutical industry are particularly welcomed. Articles are available online when ready, making publication as fast as possible, and include unlimited free colour illustrations, movies and other enhancements. The editorial process is completely electronic with respect to deposition, submission, refereeing and publication.

Crystallography Journals **Online** is available from [journals.iucr.org](http://journals.iucr.org)

C. Abad-Zapatero,<sup>a,b,\*</sup>  
R. Oliete,<sup>a,c</sup> S. Rodriguez-  
Puente,<sup>a,c</sup> J. Pous,<sup>a,d</sup>  
L. Martinelli,<sup>d</sup> M. E. Johnson<sup>b</sup> and  
A. Guasch<sup>a,c,e\*</sup>

<sup>a</sup>Plataforma Automatitzada de Cristal·lografia, Barcelona, Spain, <sup>b</sup>Center for Pharmaceutical Biotechnology, University of Illinois at Chicago, Chicago, Illinois, USA, <sup>c</sup>Parc Científic de Barcelona, Barcelona, Spain, <sup>d</sup>Institute for Research in Biomedicine, Barcelona, Spain, and <sup>e</sup>Institut de Biologia Molecular de Barcelona–CSIC, Barcelona, Spain

Correspondence e-mail: caz@uic.edu,  
aguasch@pcb.ub.cat

Received 27 June 2011

Accepted 18 August 2011

## Humidity control can compensate for the damage induced in protein crystals by alien solutions

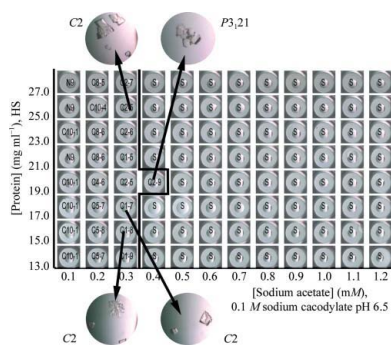
The use of relative humidity control of protein crystals to overcome some of the shortcomings of soaking ligands (*i.e.* inhibitors, substrate analogs, weak ligands) into pre-grown apoprotein crystals has been explored. Crystals of PurE (EC 4.1.1.21), an enzyme from the purine-biosynthesis pathway of *Bacillus anthracis*, were used as a test case. The findings can be summarized as follows: (i) using humidity control, it is possible to improve/optimize the diffraction quality of crystals soaked in solutions of organic solvent (DMSO, ethanol) containing ligands/inhibitors; (ii) optimization of the relative humidity can compensate for the deterioration of the diffraction pattern that is observed upon desalting crystals grown in high salt; (iii) combining desalting protocols with the addition of PEG it is possible to achieve very high concentrations of weak ligands (in the 5–10 mM range) in soaking solutions and (iv) fine control of the relative humidity of crystals soaked in these solutions can compensate for the deterioration of crystal diffraction and restore ‘high-resolution’ diffraction for structure-based and fragment-based drug design. It is suggested that these experimental protocols may be useful in other protein systems and may be applicable in academic or private research to increase the probability of obtaining structures of protein–ligand complexes at high resolution.

### 1. Introduction

The notion and observation that the diffraction pattern of protein crystals changes with the humidity of the medium surrounding the crystals dates back to the first diffraction of protein crystals by Bernal & Crowfoot (1934) and was a crucial insight for the development of the field (Abad-Zapatero, 2005). It was also systematically studied by Perutz in his early attempts to solve the phase problem by studying the shrinkage of hemoglobin crystals in different salt solutions (Perutz, 1946). In recent years, the availability of devices that permit fine control of the relative humidity of the crystals [free-mounting systems (FMS) or humidity-control (HC) devices; Kiefersauer *et al.*, 2000; Sanchez-Weatherby *et al.*, 2009] has made it possible to improve the resolution (in some cases dramatically) of protein crystals whose diffraction properties were suboptimal. The current status of these developments in macromolecular crystallography have recently been reviewed (Russi *et al.*, 2011), particularly in relation to the methodology used in fragment-based approaches to the discovery of lead compounds (Böttcher *et al.*, 2011).

Critical to any structure-based drug-design (SBDD) effort, and more so for fragment-based approaches (FBDD), is the availability of large numbers of target–ligand (target–fragment) complexes that can be used to validate the initial ‘hits’ or to optimize valuable lead compounds by medicinal chemistry efforts. Yet, it is a common observation that well diffracting protein crystals deteriorate significantly and often also rapidly upon soaking with concentrated solutions of the fragment or ligand compounds typically dissolved in dimethyl sulfoxide (DMSO).

In addition, fragment-based approaches for drug discovery and even conventional SBDD protocols quite often encounter difficulties in introducing ligands either by soaking or cocrystallization of low-



© 2011 International Union of Crystallography  
All rights reserved

**Table 1**

Crystallization conditions for the different crystal forms of PurE presented in this work.

Crystal form	Buffer	Salt	PEG
A	0.1 M cacodylate pH 6.5	0.75 M sodium acetate	—
B	0.1 M Tris pH 8.5	0.3 M sodium acetate	15% 4K
C	0.1 M Tris pH 7.5	0.8 M sodium formate	15% 4K
D	0.1 M Tris pH 7.5	0.8 M sodium formate	10% 1K, 10% 8K
E	0.1 M cacodylate pH 6.5	0.3–0.4 M sodium acetate	—

affinity compounds. During the soaking process, this is often because the active sites of the targets of interest are occupied by salts, additives or other chemicals that preclude or prevent successful soaking of target–ligand complexes (Böttcher *et al.*, 2011). Although it might appear that cocrystallization can address this problem, most of the time this is not the case because the ligands typically have weak affinity (in the 10–100  $\mu$ M range) and have to compete with the presence of high concentrations of salts (>0.5 M) that are required to crystallize the proteins. Thus, even in cocrystallization experiments the putative target–ligand complexes do not result in satisfactory crystallization outcomes. Research groups trying to soak/cocrystallize substrate analogs, cofactors and other compounds of interest in order to study enzymatic mechanisms often encounter similar problems.

The purpose of the work described here was to test whether fine control of the relative humidity of the crystals could be used to address some of the above issues and limitations. In practical terms, we wanted to establish experimental protocols that would increase the positive outcome of experiments designed to introduce ligands into pre-grown apoenzyme crystals. The experiments were designed to (i) recover the quality of the diffraction pattern of the crystals after ligand soaking, (ii) diminish the presence of salts (or other interfering chemicals) in the active sites of proteins to facilitate the binding of weak ligands and (iii) maximize the effective concentration of weak ligands in the soaking solutions to facilitate the validation of fragment-based approaches.

In addition, we systematically explored crystallization protocols under low-salt conditions, beyond the optimized initial screens, in an attempt to find different crystal forms or other favorable conditions that would be more amenable to successful soaking experiments. For this purpose, we used systematic searches in ‘protein crystallization space’, also called ‘phase diagrams’ (Saridakis *et al.*, 1994) or in more practical terms referred to as ‘precipitation diagrams’ (Saijo *et al.*, 2005).

As a test system, we used protein crystals of PurE (EC 4.1.1.21), a critical enzyme of the purine-biosynthetic pathway in *Bacillus anthracis* (Samant *et al.*, 2008). The structure of this enzyme expressed in *Escherichia coli* has been solved (Mathews *et al.*, 1999) at 1.5 Å resolution (PDB entry 1qcz) as well as that of a PurE–mononucleotide complex (PDB entry 1d7a), and a high-resolution (1.8 Å) structure of PurE from *B. anthracis* has also been reported (Boyle *et al.*, 2005; PDB entry 1xmp). Owing to its critical role in the growth of bacteria in human blood (Samant *et al.*, 2008), the structures of enzymes from the purine-biosynthesis pathway have been extensively studied (Zhang *et al.*, 2008) and the three-dimensional structures of PurE from several important pathogens have recently been reported (PDB entries 3rg8, 3rgg, 3oow, 3lp6, 3kuu and 3k5h; Tranchimand *et al.*, 2011; Thoden *et al.*, 2010). The crystal forms that we have obtained for the PurE from *B. anthracis* have not been reported to date and we have described and characterized these novel crystal forms as a demonstration of the importance of searching systematically in protein-crystallization space.

Our results with this enzyme system suggest that it is possible to compensate for the damage induced in protein crystals by extraneous (non-mother-liquor) solutions by suitable adjustment of the relative humidity. Whether or not these initial results can be extended or generalized to other protein systems remains an open question. If confirmed, these results could have application in the more successful preparation of crystalline protein–ligand complexes for enzymatic and structural studies in academic laboratories or in the pharmaceutical industry.

## 2. Materials and methods

### 2.1. Sample preparation

**2.1.1. Protein expression.** A plasmid with the gene encoding PurE (Q81ZH8) from *B. anthracis* with an N-terminus with the sequence MGSSHHHHHSSGLVPRGSH was prepared by the group at the University of Illinois at Chicago (UIC) as part of a collaborative agreement. The corresponding molecular weight for this plasmid is 19 205 Da.

*E. coli* BL21 transformant cells were cultured at 310 K in 500 ml TB (Terrific Broth) medium containing 500  $\mu$ l ampicillin (100 mg ml<sup>-1</sup>) and shaken (160 rev min<sup>-1</sup>) for 2–3 h to an OD<sub>600 nm</sub> of 0.6–0.7, at which point expression was induced by 1 mM isopropyl  $\beta$ -D-1-thiogalactopyranoside (IPTG). The cells were grown for an additional 4–5 h at 310 K, after which they were recovered by centrifugation.

**2.1.2. Protein purification.** An initial purification protocol was provided by the group at UIC and was subsequently optimized. The cells were resuspended in 50 mM Tris–HCl pH 8.0, 500 mM NaCl, 10 mM imidazole, one protease-inhibitor cocktail tablet, 1 mg ml<sup>-1</sup> lysozyme, 1% Triton-X and lysed by ultrasonication followed by centrifugation to obtain a soluble fraction. The soluble fraction was loaded onto a nickel immobilized metal-affinity column (HisTrap HP, GE Healthcare) and the protein was eluted using an imidazole gradient from 10 to 500 mM in 500 mM NaCl, 50 mM Tris–HCl pH 8.0.

Further purification was carried out using a Superdex 200 HiLoad 26/60 size-exclusion column which was equilibrated at 0.2 ml min<sup>-1</sup> with two different ionic buffers: high salt (200 mM NaCl, 0.05 M Tris pH 7.5) and low salt (50 mM NaCl, 0.05 M Tris pH 7.5). The two different protein salt concentrations were kept separated and are referred to as HS and LS. The protein was eluted as a unique peak that corresponded to 158 000 Da. The pure protein was kept at 277 K for short periods.

**2.1.3. Protein crystallization.** Initial crystallization conditions were identified by robot-assisted vapor-diffusion experiments using sparse-matrix screens. Experiments were performed mixing crystallization condition and sample in a 1:1 ratio to give a final volume of 200 nl. Around 1000 conditions were tested and crystals grew under four conditions at a temperature of 293 K. These conditions were subsequently scaled up and optimized at 293 K in 24-well Cryschem plates (Hampton Research, USA). The conditions were A (0.1 M cacodylate pH 6.5, 0.75 M sodium acetate), which was called the ‘salt’ condition, B (0.1 M Tris pH 8.5, 15% PEG 4000, 0.3 M sodium acetate), C (0.1 M Tris pH 7.5, 15% PEG 4000, 0.8 M sodium formate) and D (0.1 M Tris pH 7.5, 10% PEG 1000, 10% PEG 8000, 0.8 M sodium formate). The three latter conditions were called ‘salt + PEG’ conditions. Form E was found much later after exploring a wide range of salt and protein concentrations through the protein precipitation diagram. The details are summarized for convenience in Table 1 and the crystallographic parameters, packing ratios and data-

**Table 2**

Unit-cell parameters and data-collection statistics for the different crystal forms of PurE presented in this work.

Values in parentheses are for the last resolution shell.

Crystal form	Space group	Unit-cell parameters (Å, °)	$R_{\text{merge}}$ (%)	Completeness (%)	Beamline	$\langle I/\sigma(I) \rangle$	Multiplicity	No. of unique reflections	Resolution limits (Å)	Matthew coefficient (Å <sup>3</sup> Da <sup>-1</sup> )	Solvent content (%)	AU†
<i>A</i>	<i>P</i> 3 <sub>1</sub> 21	<i>a</i> = <i>b</i> = 86.86, <i>c</i> = 131.37	5.4 (32.0)	99.9 (99.9)	ESRF ID14-1	29.2 (7.2)	10.9 (10.4)	57662	28.5–1.76 (1.80–1.76)	1.86	33.92	4
<i>B</i>	<i>P</i> 6 <sub>2</sub> 22	<i>a</i> = <i>b</i> = 87.00, <i>c</i> = 270.00	7.1 (31.0)	96.6 (94.1)	ESRF ID14-2	32.7 (5.8)	8.1 (6.0)	42925	50–1.95 (2.05–1.95)	1.92	35.93	4
<i>C</i>	<i>P</i> 6 <sub>2</sub> 22	<i>a</i> = <i>b</i> = 88.20, <i>c</i> = 275.26	7.0 (47.5)	72.5 (50.4)	Rigaku MicroMax-007	16.5 (1.9)	3.1 (1.9)	9821	50–3.00 (3.10–3.00)‡	2.01	38.84	4
<i>D</i>	<i>P</i> 6 <sub>2</sub> 22	<i>a</i> = <i>b</i> = 87.12, <i>c</i> = 269.15	8.1 (17.1)	98.6 (92.0)	Rigaku MicroMax-007	39.0 (13.3)	9.1 (8.6)	12902	50–2.99 (3.10–2.99)‡	1.92	35.90	4
<i>E</i>	<i>C</i> 2	<i>a</i> = 87.56, <i>b</i> = 151.90, <i>c</i> = 134.85, $\beta$ = 98.33	7.3 (43.4)	93.4 (89.5)	ESRF ID14-2	38.2 (8.9)	5.1 (5.2)	56146	50–2.50 (2.56–2.50)	1.92	36.08	12

† Number of chains in the asymmetric unit. 4 refers to a full tetramer and 12 corresponds to a full octamer and an additional tetramer in the monoclinic *C*2 cell. ‡ Data collection in-house using a rotating anode at room temperature; all other data were collected on the ESRF synchrotron beamlines under cryoconditions after the crystals had been adjusted to the optimal r.h. and frozen by dismounting as described in §2.

collection statistics of the different crystal forms are presented in Table 2.

**2.1.4. Exploration of the precipitation diagram.** A program was designed to explore the precipitation diagram of PurE using a nanolitre-handling dispensing device. Phase-diagram experiments for the successful crystallization conditions were performed using a Cartesian Dispensing System (Genomic Solutions, UK). The program was designed for 96-well MRC plates (Swissci, Switzerland). The experiments were designed as follows. Firstly, the protein was dispensed into the plate, decreasing the volume along each row. The protein buffer was then added above the sample in order to reach the same volume for each well. The concentration of the precipitant increased from left to right. An example plate is shown in Fig. 1. In form *A* the sodium acetate range varied between 0.2 and 0.6 *M*. In forms *C* and *D* the sodium formate ranges were between 0.005 and 1.2 *M*, keeping the PEG concentration constant, while the concentration of PEG varied between 15 and 21%, keeping the sodium formate concentration constant. In all forms (*A*, *B*, *C* and *D*) pH variation (5.4–8.5) was performed following the same protocol.

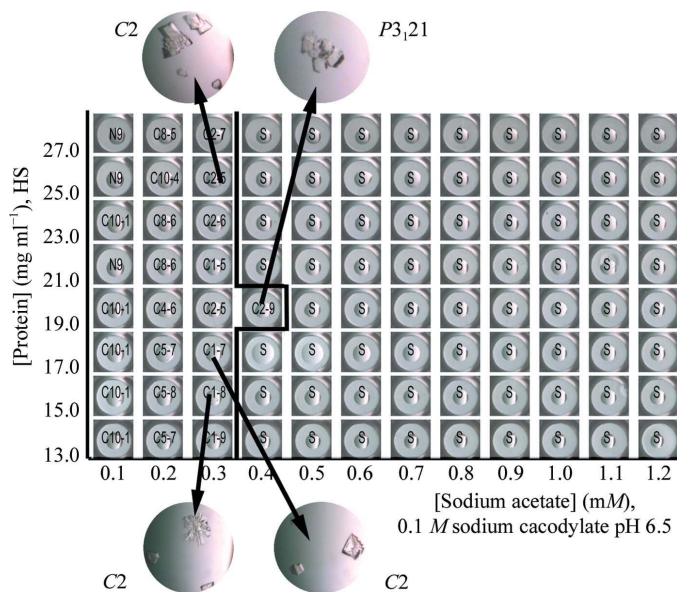


**Figure 1**

Precipitation diagram of PurE protein (form *A*) versus salt concentration. The symbols were assigned by the appearance of nuclei (N), crystals (C) and clear drops (S). In order to attempt a quantitative assessment, two additional codes were assigned (CX–Y). X: 1–10 for number of crystals. Y: 1–10 for quality, 10 being the best.

**2.1.5. Soaking of protein crystals.** Standard soaking protocols were as follows. 1  $\mu$ l of a concentrated stock solution (100 mM) of the ligand (most commonly in DMSO) was mixed with 19  $\mu$ l of the crystal mother liquor. This protocol limits the exposure of the protein crystals to the damaging effect of DMSO (5%) and maximizes the exposure of the protein crystal to the ligand (5 mM). The affinity of the ligands (*i.e.* substrate analogs, inhibitors and fragment libraries) could be in the micromolar range but would certainly be weaker if the soaking ligands were small fragments. Typical soaking times can range from a few (4–6) hours to overnight (1 ovn; 14–16 h) or longer soaks (2 ovn; ‘two overnights’, 28–32 h). Longer soaks maximize the exposure of the crystals to the ligands but result in damage to the crystals, which lose their diffraction qualities. Soaking experiments that maximize the ligand exposure under very low salt concentrations are described below.

**2.1.6. Sequential desalting protocols.** Specific protocols were designed in order to maximize the ligand concentration in the solution while at the same time minimizing the presence of salt in the mother liquor. Sequentially, the salt concentration was decreased in the crystal while the PEG concentration was increased and at the same time a high-concentration solution of the ligand in ethanol or DMSO was introduced. Five different harvesting solutions, with variations in salt, PEG and ligand, were prepared. The protocols are listed in Table 3 and summarized pictorially in Fig. 2.

## 2.2. Data collection and crystallographic analysis of different crystal forms

**2.2.1. Rotating anode.** The crystals grew to full size in approximately one week and were transferred to cryoprotection buffer with an added or increased PEG concentration and flash-cooled in micromounts (MiTeGen, Ithaca, USA). Native X-ray diffraction data were collected from a single crystal at 100 K using a MAR 345 detector coupled to a Rigaku MicroMax-007 rotating-anode X-ray generator (Cu  $K\alpha$  radiation) operating at 40 kV and 20 mA and equipped with Osmic confocal focusing optics (Rigaku-MSO, Texas, USA). For room-temperature data collection (295 K), 90 frames of data were collected using an oscillation angle of 1°, a crystal-to-detector distance of 200 mm and 5 min exposure time.

**2.2.2. Synchrotron data collection.** Following the different soaking protocols, the relative humidity was optimized by examining the extent and quality of the diffraction pattern visually. At the optimal diffraction pattern, room-temperature data sets were collected, typically using 1° oscillation and exposure times ranging from 0.1 to 0.5 s for a maximum of 120°. In addition, in certain cases and for certain conditions crystals were frozen at the optimal relative

humidity by dismounting them into the standard sample exchangers. Full data sets at high resolution were subsequently collected on different beamlines when time was available. X-ray data were collected for the apoenzyme and different soaking experiments on beamlines ID14-1 ( $\lambda = 0.9340 \text{ \AA}$ ), ID14-2 ( $\lambda = 0.9330 \text{ \AA}$ ), ID23-1 ( $\lambda = 0.9792 \text{ \AA}$ ) and BM14 ( $\lambda = 0.97625 \text{ \AA}$ ) at the ESRF. Details are provided in Table 2.

**2.2.3. Humidity-control devices.** Two different devices were used to control the relative humidity in two separate installations. Firstly, the original system design referred to as a free-mounting system (FMS; Kiefersauer *et al.*, 2000) was used. This instrument achieves dehydration by two airstreams of 0% and 100% relative humidity (r.h.) that are mixed giving the desired r.h. A feedback mechanism based on dew-point measurement is used to determine the actual r.h., which depends on the temperature of the sample. Variations in r.h. are achieved by software control of the two independent streams. The device was adapted and installed in an in-house Rigaku X-ray generator as presented above.

The second device, described as a humidity-control (HC) device, is based on the nozzle of a standard cryostream (Sanchez-Weatherby *et al.*, 2009) and can be rapidly and easily installed on different beamlines if they are already equipped with the appropriate mounting. The experimental protocols varying the r.h. were performed on the ESRF synchrotron-radiation beamline BM14, but the unit is easily transportable to other beamlines (*i.e.* ID23-1). The data sets collected on BM14 used a wavelength of  $0.97625 \text{ \AA}$ . Conveniently, once the optimal relative humidity has been obtained, the crystals can be frozen by dismounting them into a standard sample exchanger for future data collection at 100 K. These protocols were used on ESRF beamlines ID14-1, ID14-2 and ID23-1 for the collection of full data sets under cryoconditions.

**2.2.4. Data processing.** Indexing and characterization of the different crystal forms was performed with the interactive *iMOSFLM* package (Battye *et al.*, 2011) using the automatic indexing routine. Selection of the most suitable unit-cell parameters and crystallographic symmetry was performed by selecting the parameters corresponding to the highest possible symmetry and lowest possible penalty. Similar strategies were used when the data were processed with *HKL-2000* (Otwinowski & Minor, 1997).

**Table 3**  
Details of the soaking protocols of apo PurE crystals for desalting and optimization of ligand concentration.

(a) Form *D* soaking protocols.

Solution No.	Tris pH 7.5 (M)	PEG 8K [% (w/v)]	PEG 1K [% (w/v)]	Sodium formate (M)	L3† compound (mM)	Soaking time
1	0.1	12	10	0.40	No	15 min
2	0.1	14	10	0.20	No	15 min
3	0.1	16	10	0.05	7.45	15 min
4	0.1	18	10	0.01	14.90	15 min
5	0.1	20	10	0	29.81	1 or 2 ovr

(b) Form *C* soaking protocols.

Solution No.	Tris pH 7.5 (M)	PEG 4K [% (w/v)]	Sodium formate (M)	L1† compound (mM)	Soaking time
1	0.1	17	0.4	No	15 min
2	0.1	19	0.2	No	15 min
3	0.1	21	0.05	2.89	15 min
4	0.1	23	0.01	5.78	15 min
5	0.1	25	0	11.56	1 or 2 ovr

† L1 and L3 refer to small fragments in the ActiveSight library. The final concentration of the ligands depends on the solubility of the ligands. Initial conditions ('mother liquor') are as indicated in Table 1 for the corresponding forms.

**2.2.5. Structure solution and refinement.** The structures of PurE in high-symmetry forms (hexagonal and trigonal) diffracting to high resolution (forms *A* and *B*) were solved by molecular replacement using the coordinates of *B. anthracis* PurE (PDB entry 1xmp) as a search model after removing all solvent atoms. Molecular replacement was performed using *MOLREP* (Lebedev *et al.*, 2008; Vagin & Teplyakov, 2011) from the *CCP4* (Winn *et al.*, 2011) suite of programs. Cross-rotation and translational searches for one tetramer in the asymmetric unit (subunits *A–D*) were performed with data from 15 to 3.0 Å resolution, followed by rigid-body refinement with *REFMAC5* (Murshudov *et al.*, 2011). The model was rebuilt manually using  $\sigma_A$ -weighted  $2mF_o - DF_c$  and  $mF_o - DF_c$  electron-density maps with the *Coot* (Emsley & Cowtan, 2004) molecular-graphics program while gradually introducing higher resolution reflections up to the resolution limit. An initial set of water molecules were located with *Coot*

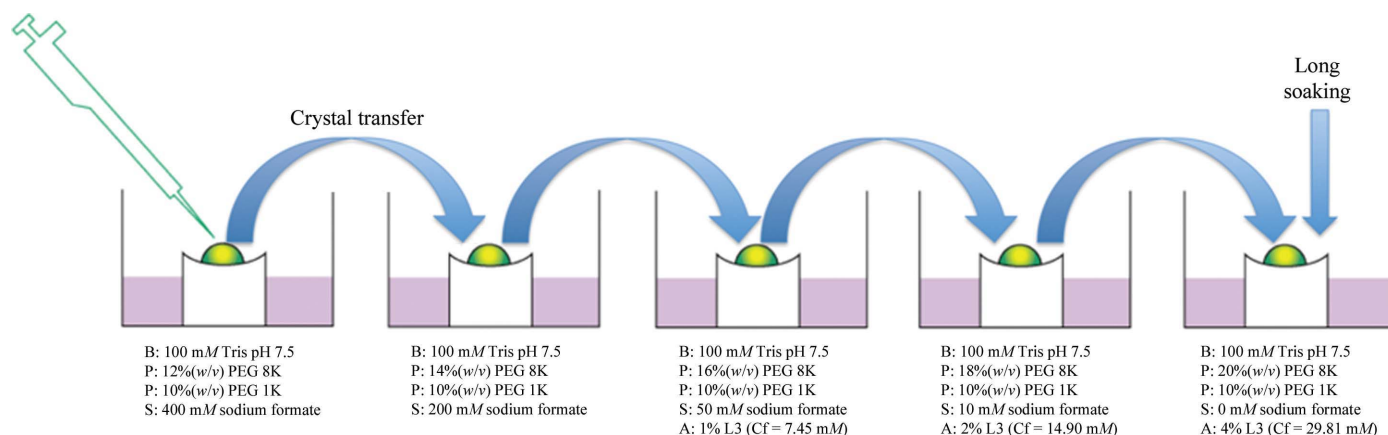


**Figure 2**

Pictorial summary of the soaking protocols. The diagram illustrates the steps suggested for changing the initial mother liquor of the crystal to a solution containing no salt and a high concentration of the ligand. B is the original buffer solution. P denotes the concentration of two different PEGs, one of which (PEG 8K) changes progressively from 12 to 20%. The concentration of PEG 1K remains constant at 10% (w/v). S denotes the salt solution, which changes from the initial 0.4 M sodium formate to 0.0 M (see Tables 1 and 3 for crystallization conditions *versus* soaking protocols). A indicates the solution containing the ligand at the corresponding percentage (v/v) to a final concentration of 29.81 mM. The solvent for the ligand can be DMSO or ethanol.

and were refined with *REFMAC5* (Murshudov *et al.*, 2011). The current refinement statistics for these two forms are  $R_{\text{work}} = 0.183$ ,  $R_{\text{free}} = 0.231$  ( $P3_121$ ) and  $R_{\text{work}} = 0.173$ ,  $R_{\text{free}} = 0.214$  ( $P6_522$ ).

The monoclinic  $C2$  crystal form (form *E*) was solved using a similar strategy and a definitive solution was found with three independent tetramers in the asymmetric unit. This solution was later reconfigured to a full octamer in a general position and a tetramer near a crystallographic twofold. This structure has also been partially refined using the same strategy as above and the current refinement statistics are  $R_{\text{work}} = 0.173$  and  $R_{\text{free}} = 0.250$ . Exhaustive refinement of the solvent structures in the three forms is continuing.

### 3. Results and discussion

Initial crystallographic screens yielded two basic crystal forms: hexagonal ( $P6_522$ ) and trigonal ( $P3_121$ ) (Table 2). The hexagonal form was the predominant form under various different conditions, but none of these crystal forms have previously been characterized for PurE from *B. anthracis*. The trigonal form was unique in that it only grew in the presence of high salt (0.75 *M* sodium acetate) without PEG. The type *A* crystals belonged to the trigonal space group  $P3_121$ , with unit-cell parameters  $a = b = 88.9$ ,  $c = 133.4$  Å.

The crystals of forms *B*, *C* and *D* were all hexagonal and belonged to space group  $P6_522$ , with unit-cell parameters of approximately  $a = b = 87.4$ ,  $c = 276.0$  Å. Although grown using different precipitant salts (sodium acetate *versus* sodium formate) and at different concentrations (0.3 *versus* 0.8 *M*) and different pHs (8.5 *versus* 7.5), these three forms appeared to be isomorphous based on their closely similar unit-cell parameters, particularly forms *B* and *D*. A summary of the various crystal forms characterized and analyzed in this study is presented in Table 2. Interestingly, the unit-cell volume of the hexagonal form is approximately double that of the trigonal form. This dramatic change is achieved by approximately doubling the  $c$  axis while retaining the same dimensions for the shorter axes ( $a = b \simeq 88$  Å). The unit-cell parameters of the  $C2$  cell correspond approximately to a re-indexing of the trigonal cell with the  $C222$  equivalent orthorhombic cell of dimensions  $a = 88$ ,  $b = 152.4$ ,  $c = 132$  Å after changing the orthogonal angle of the cell to  $\beta = 98.33^\circ$  for the monoclinic cell. This observation suggests that the crystal packings of the different crystal forms are related (see below).

Previous work revealed that the structure of the enzyme from *B. anthracis* was an octamer exhibiting 422 symmetry (Boyle *et al.*, 2005). The octamer also crystallized in a  $C2$  cell and the crystal contained a full octamer in the asymmetric unit. Structure solution of the forms diffracting to high resolution (forms *A*, *B* and *E*; see §2)

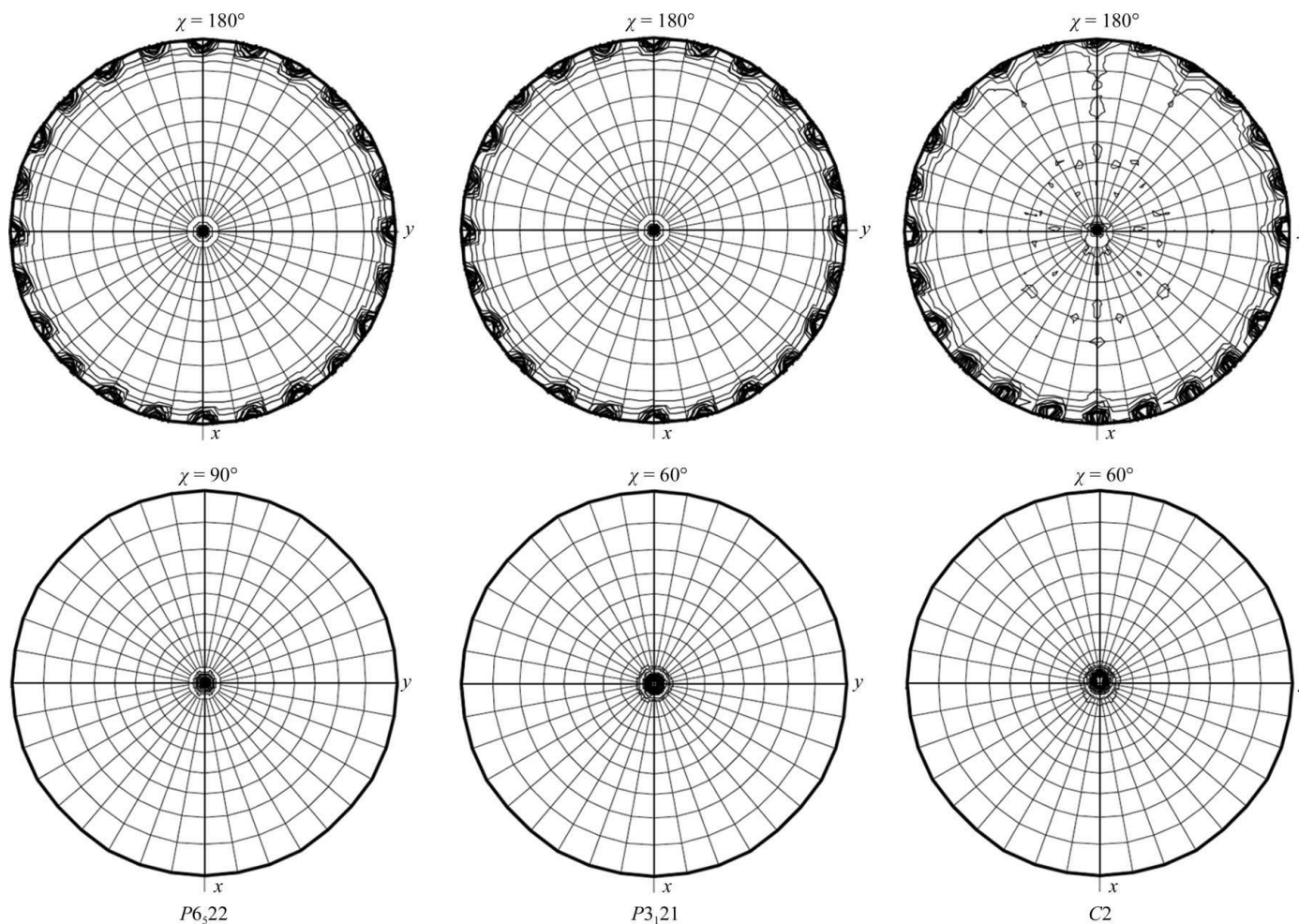


**Figure 3** Self-rotation functions of the three different crystal forms of PurE. The top panels (left to right) present the planes for twofolds ( $\chi = 180^\circ$ ) for the three different forms ( $P6_522$ ,  $P3_121$  and  $C2$ , respectively). The lower panels depict the planes for the orientation of the fourfold of the PurE octameric aggregate (left;  $\chi = 90^\circ$ ) in the  $P6_522$  form, the crystallographic packing symmetry of the  $P3_121$  form (center) and the analogous packing symmetry of the  $C2$  form (right).

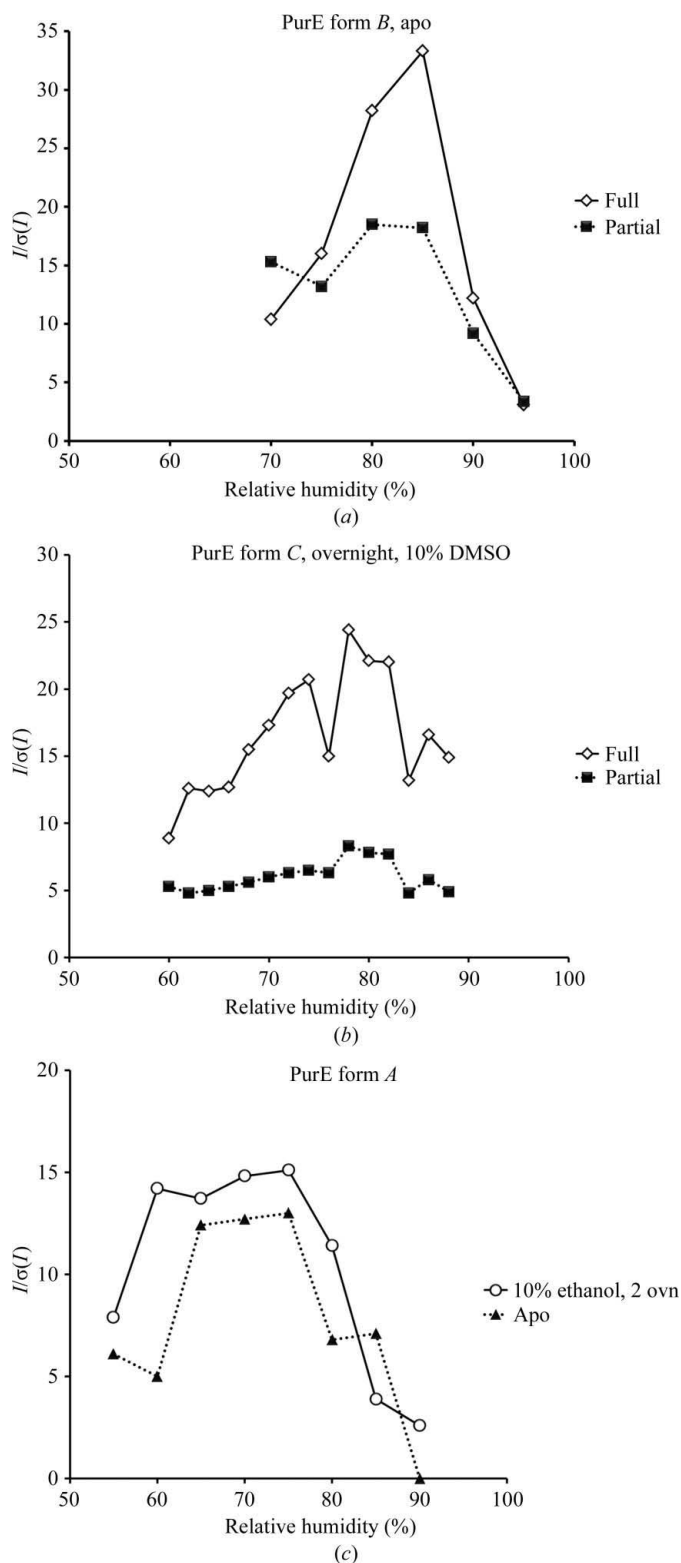


**Figure 4**  
Quantitative analysis of the improvements in the diffraction pattern in relation to r.h. (a) Mean  $I/\sigma(I)$  versus relative humidity for the apo crystals of PurE form B. Open diamonds refer to full reflections and black squares refer to partials. An optimum is seen at approximately 85% r.h. (b) As in (a) for crystals of PurE form C soaked in 10% DMSO overnight. (c) Comparison of the diffraction quality, mean  $I/\sigma(I)$ , versus r.h. of PurE crystals (form A). Open circles refer to crystals soaked in 10% ethanol for 2 ovn. Black triangles refer to apo crystals. Mean  $I/\sigma(I)$  refers to the  $I/\sigma(I)$  values for all reflections at the maximum [ $I/\sigma(I) > 2.0\sigma$ ] resolution of the diffraction pattern.

revealed that the three forms had basically the same packing arrangement of the PurE octamer particle. The packing arrangement can be briefly described as the hexagonal closest packing of a 422 aggregate in a hexagonal arrangement. The particle fourfold axis is parallel to the high-symmetry crystallographic axis in the trigonal and hexagonal forms that coincides with the  $c^*$  direction of the  $C2$  cell (Fig. 3). The center of the PurE octamer does not coincide with the position of the high-symmetry axes. The perpendicular crystallographic dyads in the high-symmetry forms spaced by 30–60° correspond to similar noncrystallographic twofolds in the  $C2$  form in the  $ab$  plane (Fig. 3). The combination of the particle symmetry and the crystallographic symmetry also produces noncrystallographic dyads at 15–45° intervals that are also apparent in the  $C2$  form. It should be mentioned that the  $C2$  packing of this structure is different from that observed by previous investigators and the  $V_M$  values are also different (1.9 versus 2.2 Å<sup>3</sup> Da<sup>-1</sup>; Boyle *et al.*, 2005). Based on our preliminary analysis of the current refined structures, the different crystal forms arise from the different extents of ordering of the

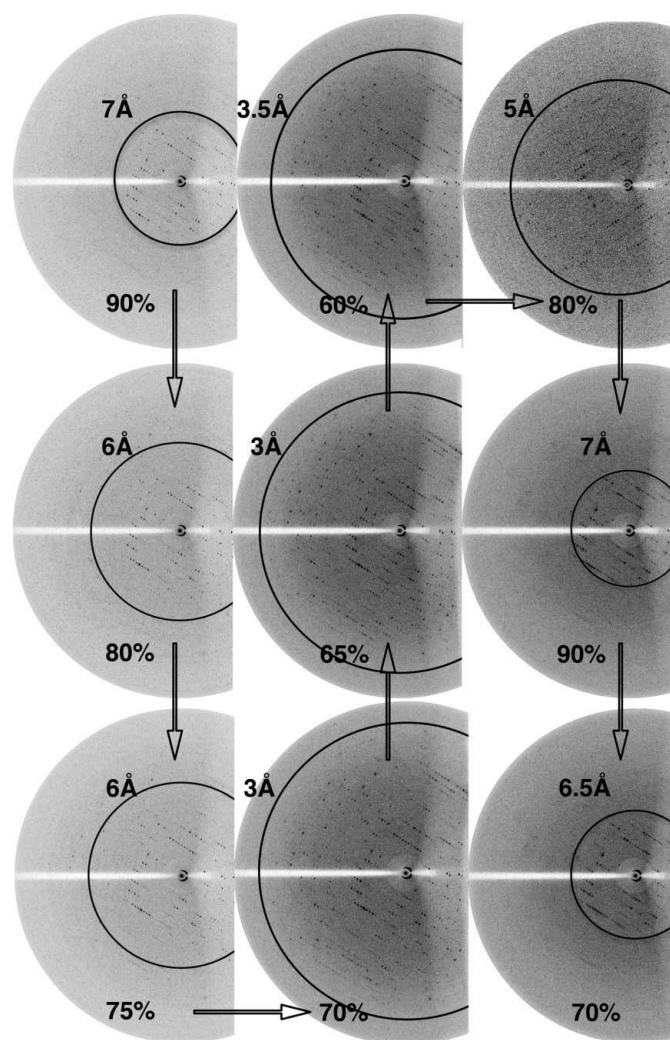


**Figure 5**  
Effect on the diffraction pattern of changes in the relative humidity of crystals of PurE after soaking for 1 ovn in 5% DMSO (form A). Arrows indicate the sequence of the r.h. changes. The experiment was conducted with the FMS installed on the in-house rotating anode as described in §2.2.3. The collage is made up of images directly obtained from the FMS, in which the right-hand portion of the detector is partly shaded by the mechanical jacket containing the airflow hoses (Kiefersauer *et al.*, 2000).

carboxy-terminal residues (Glu156-Gly157-Ser158-Glu159-Leu160-Val161) of the subunits in the external contact areas of the octamer. Further details will be provided in a future publication.

The similar packing arrangement described above and the corresponding change in unit-cell parameters is reflected in similar solvent contents and packing ratios for the three forms (Table 2). The crystal symmetry that was most versatile from the viewpoint of plasticity for variation of the humidity control turned out to be the hexagonal one corresponding to forms *B*, *C* and *D*. We attribute this plasticity to the presence of various types and amounts of PEG in the crystallization mixture that do not interact specifically with the macromolecules in the crystal as has been observed by other researchers (Böttcher *et al.*, 2011) and provide a ‘cushion’ for the subtle changes in the intermolecular contacts of the crystal. These PEG-containing forms were the crystals that we have used most extensively for the optimization of protocols designed to soak ligands into pre-grown apoenzyme crystals. Except for form *B*, which grows at 0.3 *M* sodium acetate, the other two high-symmetry forms (forms *C* and *D*) grow at rather high formate concentration (0.8 *M*). Form *E* was found through systematic screening of the precipitation diagram (also referred to as the phase diagram), varying the protein concentration, the salt concentration and the pH (Fig. 1). Although this crystal form belongs to the same space group as the previously reported structure of *B. anthracis* (PDB entry 1xmp) and was grown at high sodium formate concentrations, the unit-cell parameters are different and the two crystal forms are not isomorphous ( $a = 168.3$ ,  $b = 76.5$ ,  $c = 102.7$  Å,  $\beta = 96.7^\circ$ ; see Table 2). It should be noted that the clones used for the two different protein preparations differed in the N-terminal His tags that were used to facilitate protein purification (Boyle *et al.*, 2005).

The initial working protocols to establish the starting r.h. of the hexagonal crystals were those suggested in publications describing

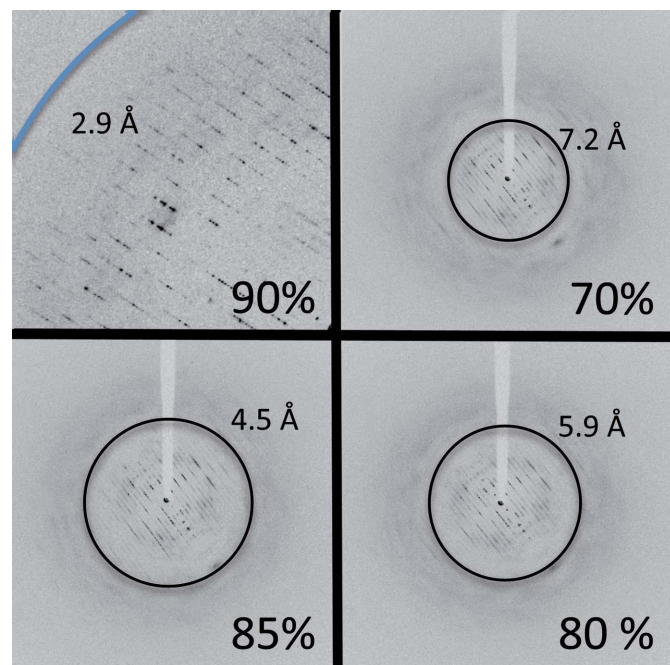


**Figure 6**

Improvements of the diffraction pattern of crystals of form *B* after desalting (0.8 *M* to 50 mM sodium formate, 8 h, PEG constant). The initial r.h. was 85% and varied counterclockwise as indicated. Other experiments varying the r.h. from 70% clockwise also had an optimum at the higher r.h. (90%). This experiment was conducted on beamline BM14 (ESRF) using the HC device (see §2).

the FMS instrument (Kiefersauer *et al.*, 2000). Firstly, using our in-house FMS we found that the hexagonal crystals of PurE were indeed sensitive to the fine control of relative humidity and that the effects were reproducible, and established that the optimum r.h. was near 85% (scale based on the instrument settings without absolute calibration; Fig. 4a). Further experiments showed that the optimum r.h. for the form *A* crystals was in the range 70–80% (Fig. 4c).

A critical factor in the diffraction quality of macromolecular crystals soaked with active ligands (inhibitors, effectors, substrate analogs *etc.*) is the perturbation of the native environment (*i.e.* mother liquor) of the crystals. This is particularly true for compounds that are poorly soluble in aqueous solutions, as is the case for the majority of chemical entities of pharmaceutical interest (Böttcher *et al.*, 2011). The solvent of choice for the preparation of stock solutions (~100 mM) is DMSO and to a lesser extent ethanol. Macromolecular crystals are typically very sensitive to low concentrations [ $\sim 5\%$  (v/v)] of these carrier solvents and the diffraction quality of the crystals deteriorates very readily upon soaking.

We have systematically tested the effect of changes in the r.h. of crystals that have been exposed to various concentrations of DMSO.

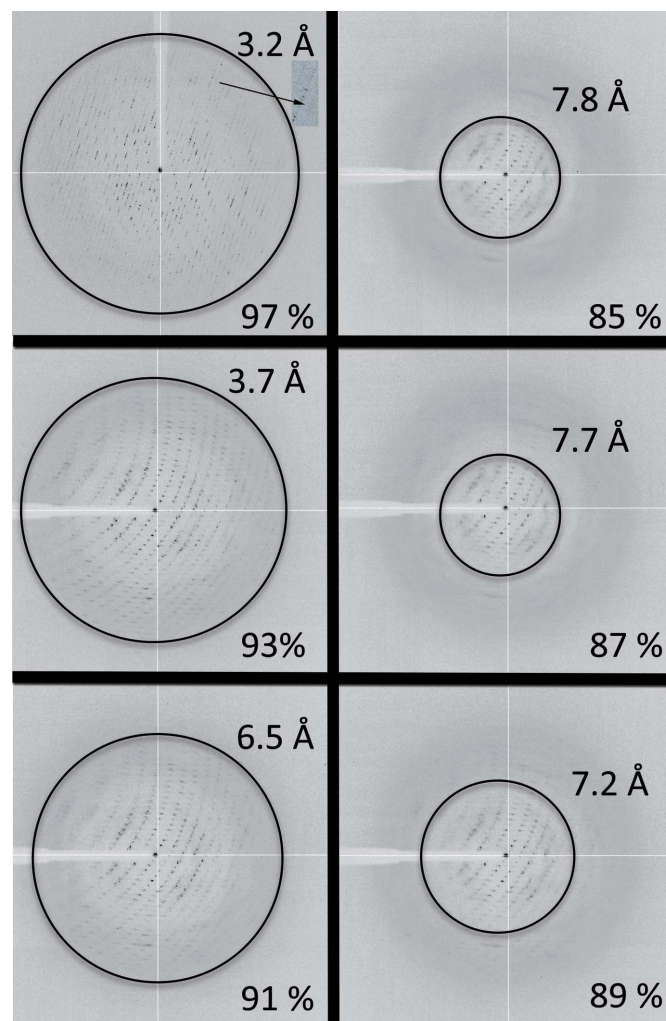


**Figure 7**

Improvements of the diffraction pattern of crystals of form *D* after lowering the salt concentration (sodium formate) from 0.8 to 0 *M* and letting them equilibrate overnight according to the protocols shown in Table 3. This experiment was conducted on beamline BM14 (ESRF). Note that with the HC device there is no blind area in the detector (as opposed to FMS; see §2, Fig. 5 *versus* Figs. 6 and 7).

The most significant results are summarized in Figs. 4 and 5. Fig. 5 visually presents the results of varying the relative humidity (90–60%) of crystals of PurE (form *A*) after soaking for long exposures (overnight in 10% DMSO). An optimum of the diffraction pattern can be appreciated visually between 65 and 70%, while for form *B* the optimum is centered near 80%. Quantitative analysis of these results is presented in Fig. 4(*b*). The effect of ethanol soaking (2 ovn) on crystals of form *A* is shown (Fig. 4*c*) compared with native apo PurE crystals. In these experiments we have selected long (>8 h) soaking times to illustrate the dramatic improvement in the quality and extent of the diffraction pattern and also because these protocols maximize the soaking time, which is an important factor for the soaking of weak ligands. In other experiments with soaking times of a few hours (1–4 h) crystal damage is not so severe and consequently the recovery effect is less striking. Although it might be crystal-dependent, it would appear that for long soaking times in ethanol the organic solvent appears to enhance the diffraction quality and resilience of these crystals upon changes in the relative humidity (Fig. 4*c*).

Also important in optimizing the soaking of ligands into crystals grown in high salt is to explore the results of lowering the salt concentration and determine whether it is possible to recover the quality and extent of the diffraction patterns by changing the relative humidity. Our observations demonstrated that it was possible to improve the diffraction pattern of form *B* crystals soaked in lower salt concentrations (50 mM) for 8 h (Fig. 6). Interestingly, the diffraction pattern improved upon raising the r.h. of the crystals from 85 to 90%; we never observed improvement on going to drier conditions (Figs. 6 and 7). The results were reproducible and it was possible to collect complete data sets (60–80° for the high-symmetry crystals) at room temperature ( $T = 297$  K) from crystals adjusted directly to the optimum r.h. (typically 96–97%; see below). Typical data-collection statistics for these data sets were  $R_{\text{merge}} \simeq 0.07$ – $0.08$  with completeness ranging from 72 to 98% for in-house experiments at a resolution

near 3 Å. The values for data sets collected from frozen crystals at the optimum r.h. were  $R_{\text{merge}} \simeq 0.048$ – $0.083$  and a completeness of 93–99.9% at resolutions of 2.5–1.76 Å (Table 2). Given the experimental facilities at the beamlines where the humidity-control instrument was set up (ESRF, BM14), crystals were frozen at the optimum relative humidity by simply dismounting them into the crystal containers under liquid nitrogen using the existing sample exchangers (see §2).

In order to maximize the exposure of the crystals to possible ligands at minimum salt concentration, we developed protocols that combined progressive ‘desalting’ solutions with higher PEG concentrations to minimize crystal deterioration. Nonetheless, standard extended soaks (1 ovn or 2 ovn) of excellent apoenzyme crystals used in soaking solutions (see §2) routinely resulted in crystals that diffracted to very low resolutions; typically 8–6 Å at best at the reference 85% relative humidity of the unsoaked crystals. Thus, it was surprising and gratifying to see that ~10% changes in the relative humidity (from 85 to 95%) restored the diffraction quality dramatically (Fig. 7). The effect was also reproducible in several crystals to the point that successive crystals from the same soaking conditions were set up directly at the optimum relative humidity (Fig. 8) and data sets were collected either at room temperature or cooled under cryoconditions on the same or a different beamline.

Following the combined protocols (desalting plus ligand soaking) described above, one can maximize the exposure of the crystals to high ligand concentrations under low (or minimum) salt concentrations; the resulting crystals also diffracted very poorly (8–7 Å resolution). Once again, relatively similar changes (~10%) in relative humidity (85–95%) restored the diffraction quality of the crystals, making them useful for data collection at room temperature (or under cryoconditions) at resolutions ranging from 2.9 to 2.3 Å (respectively) and consequently providing conclusive structural data as to the binding (or lack of binding) of the ligands. These data sets are of sufficient quality to define the binding characteristics of the

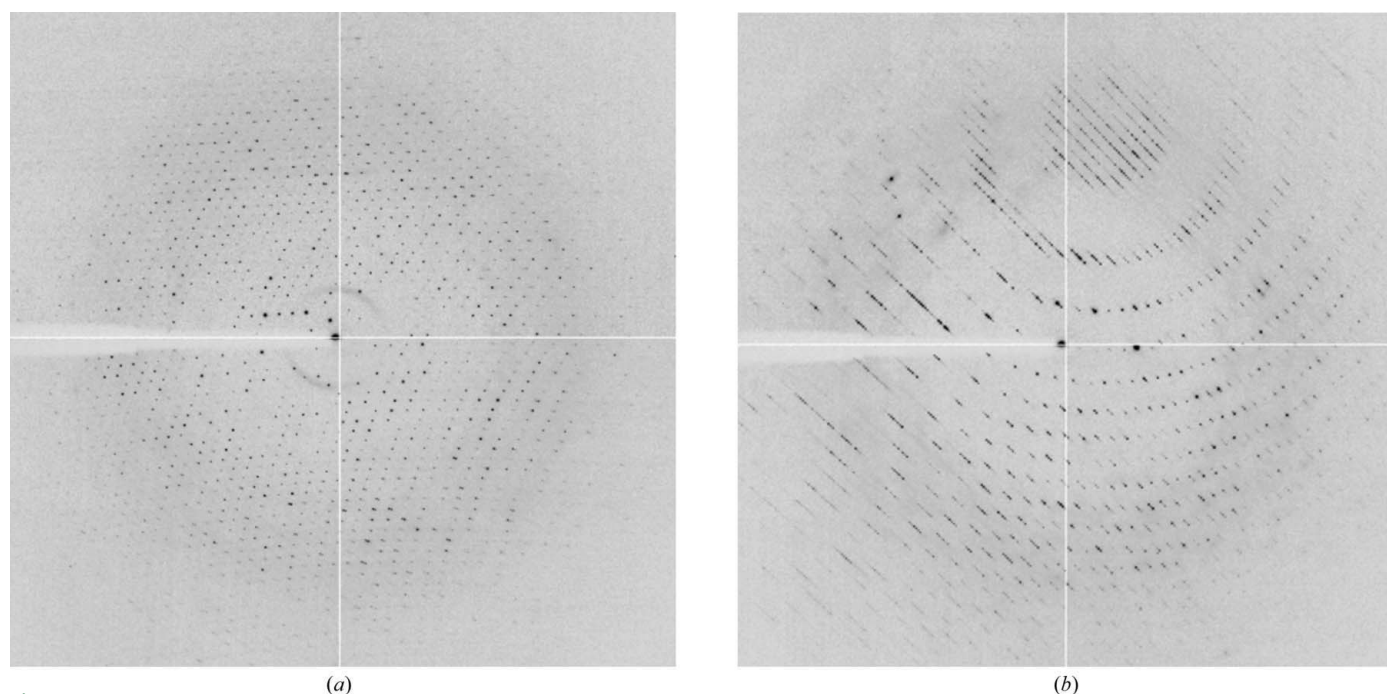


**Figure 8**

Diffraction patterns of form *D* crystals pre-soaked according to the protocols described in Table 3 and adjusted directly (no r.h. optimization) to 96% r.h. (*a*) and (*b*) correspond to  $\varphi = 0^\circ$  and  $\varphi = 90^\circ$  spindle settings, respectively. The long *c*-axis dimension is clearly appreciable with distinct fully resolved reflections. This experiment was conducted with the HC device at room temperature on beamline BM14 (ESRF).

ligand and often are acceptable to establish binding modes in mechanistic studies, hit validation or even series optimizations (Table 2).

Currently, it is common practice in experiments involving soaking of ligands into pre-grown apo crystals to use a 'harvesting solution' that is as close as possible to the mother liquor to prevent damage to the crystals. Although this approach is reasonable to maintain the integrity of the crystals and to retain their initial diffraction qualities, our results suggest that in cases where the active sites are occupied by precipitants (typically salts at high concentration) it would be advantageous to first soak the crystals in lower salt solutions. The crystals would initially diffract much more poorly, but this deterioration can be compensated by changing the relative humidity of the crystals and diffraction may successfully be restored. Alternatively, it may also be possible to soak the ligands in crystals grown in lower salt concentrations; although they might not diffract as well, the active sites could be more accessible to weak ligands. After soaking or using suboptimal crystals, the quality of the diffraction pattern could be restored by appropriate adjustment of the relative humidity of the crystals.

Our findings can be summarized as follows: (i) using humidity control it is possible to improve/optimize the diffraction quality of crystals soaked with ligands/inhibitors, (ii) optimization of the relative humidity can compensate for the deterioration of the diffraction pattern that is observed upon desalting crystals grown at high salt, (iii) combining desalting protocols with PEG addition it is possible to achieve very high concentrations of weak ligands (in the 5–10 mM range) in soaking solutions and (iv) fine control of the relative humidity of the crystals soaked under these conditions can compensate for the deterioration of crystal diffraction and restore 'high-resolution' diffraction of value for SBDD and FBDD.

Extensive exploration of the precipitation diagrams allowed us to discover the monoclinic form *E* (*C*<sub>2</sub>) at lower salt concentration (Fig. 1, Table 1), which represents a novel form and was also used for soaking of ligands and changes in relative humidity. However, it was not as suitable for room-temperature data collection because of its low symmetry. Structural details of the refined structures of PurE and the detailed solvent structures in the three different crystal lattices described above will be presented elsewhere.

The authors appreciate the support of the UIC group, in particular Drs S. Mehboob and B. Santasiero. Access to the ESRF as part of the BAG Barcelona, courtesy of Drs Miquel Coll and Ignasi Fita and the Barcelona Structural Biology community, is greatly appreciated, in particular Dr Roeland Boer for logistic support. The assistance and support of the staff of the ESRF beamlines BM14 and ID14-1

(especially Dr Silvia Rossi) in setting up the humidity-control device on various beamlines is appreciated. The financial assistance of the AGAUR agency to CA-Z for a visiting professorship at the Platform of Drug Discovery (PDD; Dr J. Quintana) is also recognized as well as the financial support of the Parc Científic Barcelona (PCB) to RO. The financial support of La Caixa Foundation to LM is appreciated. The constructive criticism of the anonymous referees is acknowledged. This work was supported in part by the Transformational Medical Technologies program contract HDTRA1-11-C-0011 from the Department of Defense Chemical and Biological Defense program through the Defense Threat Reduction Agency (DTRA).

## References

- Abad-Zapatero, C. (2005). *Acta Cryst.* **D61**, 1432–1435.
- Battye, T. G. G., Kontogiannis, L., Johnson, O., Powell, H. R. & Leslie, A. G. W. (2011). *Acta Cryst.* **D67**, 271–281.
- Bernal, J. D. & Crowfoot, D. (1934). *Nature (London)*, **133**, 794–795.
- Böttcher, J., Jestel, A., Kiefersauer, R., Krapp, S., Nagel, S., Steinbacher, S. & Steuber, H. (2011). *Methods Enzymol.* **493**, 61–89.
- Boyle, M. P., Kalliomaa, A. K., Levnikov, V., Blagova, E., Fogg, M. J., Brannigan, J. A., Wilson, K. S. & Wilkinson, A. J. (2005). *Proteins*, **61**, 674–676.
- Emsley, P. & Cowtan, K. (2004). *Acta Cryst.* **D60**, 2126–2132.
- Kiefersauer, R., Than, M. E., Dobbek, H., Gremer, L., Melero, M., Strobl, S., Dias, J. M., Soulimane, T. & Huber, R. (2000). *J. Appl. Cryst.* **33**, 1223–1230.
- Lebedev, A. A., Vagin, A. A. & Murshudov, G. N. (2008). *Acta Cryst.* **D64**, 33–39.
- Mathews, I. I., Kappock, T. J., Stubbe, J. & Ealick, S. E. (1999). *Structure*, **7**, 1395–1406.
- Murshudov, G. N., Skubák, P., Lebedev, A. A., Pannu, N. S., Steiner, R. A., Nicholls, R. A., Winn, M. D., Long, F. & Vagin, A. A. (2011). *Acta Cryst.* **D67**, 355–367.
- Otwinowski, Z. & Minor, W. (1997). *Methods Enzymol.* **276**, 307–326.
- Perutz, M. (1946). *Trans. Faraday Soc. B*, **42**, 187–195.
- Russi, S., Juers, D. H., Sanchez-Weatherby, J., Pellegrini, E., Mossou, E., Forsyth, V. T., Huet, J., Gobbo, A., Felisaz, F., Moya, R., McSweeney, S. M., Cusack, S., Cipriani, F. & Bowler, M. W. (2011). *J. Struct. Biol.* **175**, 236–243.
- Saijo, S., Sato, T., Tanaka, N., Ichiyangi, A., Sugano, Y. & Shoda, M. (2005). *Acta Cryst.* **F61**, 729–732.
- Samant, S., Lee, H., Ghassemi, M., Chen, J., Cook, J. L., Mankin, A. S. & Neyfakh, A. A. (2008). *PLoS Pathog.* **4**, e37.
- Sanchez-Weatherby, J., Bowler, M. W., Huet, J., Gobbo, A., Felisaz, F., Lavault, B., Moya, R., Kadlec, J., Ravelli, R. B. G. & Cipriani, F. (2009). *Acta Cryst.* **D65**, 1237–1246.
- Saridakis, E. E. G., Shaw Stewart, P. D., Lloyd, L. F. & Blow, D. M. (1994). *Acta Cryst.* **D50**, 293–297.
- Thoden, J. B., Holden, H. M., Paritala, H. & Firestone, S. M. (2010). *Biochemistry*, **49**, 752–760.
- Tranchimand, S., Starks, C. M., Mathews, I. I., Hockings, S. C. & Kappock, T. J. (2011). *Biochemistry*, **50**, 4623–4637.
- Vagin, A. & Teplyakov, A. (2010). *Acta Cryst.* **D66**, 22–25.
- Winn, M. D. *et al.* (2011). *Acta Cryst.* **D67**, 235–242.
- Zhang, Y., Morar, M. & Ealick, S. E. (2008). *Cell. Mol. Life Sci.* **65**, 3699–3724.